Structure Analysis of a Graphitic Boron Layer at the $TaB_2(0001)$ Surface

H. Kawanowa,[1,2] R. Souda,[1] S. Otani,[1] and Y. Gotoh[2]
[1]*National Institute for Research in Inorganic Materials, 1-1, Namiki, Tsukuba, Ibaraki 305-0044, Japan*
[2]*Department of Materials Science and Technology, Science University of Tokyo, Noda, Chiba 278-8510, Japan*
(Received 11 March 1998)

The structure of the $TaB_2(0001)$ surface has been investigated by using impact-collision Li^+ ion-scattering spectroscopy and three-dimensional three-atom computer simulation. We found for the first time that a graphitic boron layer is formed on the $TaB_2(0001)$ surface and that the scattered Li^+ ion loses significant energy due to electronic excitation when the Li^+ ion passes through the graphitic boron layer. The electronic stopping power is qualitatively explicable by the impact-parameter approximation proposed by Firsov. [S0031-9007(98)06998-1]

PACS numbers: 61.18.Bn, 68.35.Bs, 78.40.Kc, 79.20.Rf

Rare-earth and transition-metal borides (MBx) have attracted considerable attention in terms of their unique bonding and chemical properties. They are also known to be a family of high temperature materials with extreme hardness and exhibit a wide variety of electrical properties ranging from semiconducting to superconducting. All of the MBx's with boron content exceeding 40 at. % have two-dimensional or three-dimensional networks of covalently bonded boron atoms, such as graphitic layer, octahedral B_6 and icosahedral or cubo-octahedral B_{12} clusters. Despite the fact that the bulk structures of MBx have been well studied [1–5], relatively little is known about their surfaces. The surface of LaB_6 is best investigated in connection with its application as an electron emitter [6–9]; the high performance of electron emission properties arises mainly from its low work function, achieved by the termination of the La atoms interacting with the electron deficient B_6 octahedra in the second surface layer. As regards the MB_2, the boron atoms form a graphitic network sandwiched by the metal layers in bulk, and the nature of bonding of boron atoms has been discussed for past three decades in terms of whether the graphitic boron network is isoelectronic to graphite or not. Therefore, the boron-terminated MB_2 surface, if realized, is of crucial importance for better understanding the mechanism of the formation of the two-dimensional graphitic structure on surfaces. In this respect, monolayer graphite (MG) and monolayer hexagonal boron nitride (h-BN) have been studied and their unique bonding with the transition-metal substrate has been discussed [10,11]. So far, the surface structure of the $HfB_2(0001)$ and $TiB_2(0001)$ surfaces has been investigated, but it is concluded that these surfaces are terminated by the metal atoms [12,13]. Thus, the existence of B, in the form not only of the B clusters but also of independently chemisorbed B atoms, has not been reported on the MB_2 and MB_6 surfaces.

In this Letter, we investigate the atomic structure of the $TaB_2(0001)$ surface. On the basis of the impact-collision Li^+ ion-scattering spectroscopy (Li^+ ICISS) experiment, together with the computer simulation, we found for the first time that the graphitic boron layer terminates the $TaB_2(0001)$ surface. The boron atoms are located on every threefold hollow site of the hexagonal tantalum layer. For stabilizing the graphitic B layer, strong hybridization between B $2s$, $2p$, and Ta $5d$ states may be required, which provides remarkable contrast to the formation of more stable MG and monolayer h-BN on transition-metal surfaces. The ICISS results also showed marked energy loss of the scattered Li^+ ion. From careful analysis of the energy and angular dependence of the energy loss values, the Li^+ ions are found to lose their kinetic energy due to electronic stopping when they pass through the negatively charged graphitic boron layer. The Firsov theory, in which electronic stopping depends upon the impact parameter, explains the experimental result qualitatively well.

The experiments were performed in an ultrahigh vacuum (UHV) chamber (base pressure $<2 \times 10^{-8}$ Pa) equipped with He^+ and Li^+ ion sources, a photon source for ultraviolet photoelectron spectroscopy (UPS), a rotatable hemispherical electrostatic analyzer (ESA) and optics of reflection high energy electron diffraction (RHEED). The substrate was mounted on a precision manipulator via the sample transfer system. A single crystal rod of TaB_2 was grown by a floating-zone technique [14]. A substrate of 1 mm thickness was cut from the rod after the Laue alignment within 0.5° accuracy from the [0001] direction. The substrate surface was mechanically polished, with B_4C powder and diamond paste to a mirror finish. The substrate was heated in UHV by an electron bombardment from behind. The as-polished surface was first annealed up to 1500 K in 5×10^{-4} Pa of oxygen ambient for 15 min to remove the carbon contamination, and flashed subsequently up to 1500 K below 2×10^{-7} Pa to obtain a clean surface. The clean surface exhibited a sharp 1×1 pattern in RHEED and no oxygen, carbon, and other impurity peak in He-ISS. Li-ICISS was used for the surface structure analysis in order to get a better ion counting rate than He-ICISS. The 1000 eV Li^+ ions were focused on the surface with various incidence angles α (with respect to the surface), and scattered Li^+ ions through a scattering angle of 155° were detected by means of ESA with a constant energy resolution of 6 eV.

 0031-9007/98/81(11)/2264(4)$15.00

The bulk crystal of the TaB_2 has a hexagonal structure with sixfold symmetry, Ta layer and graphitelike boron layer being stacked alternately in the [0001] direction. A z axis projection of the structure is shown in Fig. 1. The ICISS spectra were taken along the $[11\bar{2}0]$ and $[10\bar{1}0]$ azimuths. The fact that the RHEED pattern of the clean $TaB_2(0001)$ surface showed a (1×1) pattern indicates that the surface structure is essentially the same as that of the bulk structure in a horizontal direction.

The narrow energy scans taken along the $[10\bar{1}0]$ azimuth at various incident angles are shown in Fig. 2(a). The binary collision energy of the 1000 eV Li^+ ion off the Ta atom is calculated at 863 eV and is indicated by an arrow in Fig. 2(a). The peaks at about 850 eV are identified as the surface peak of Li^+ scattered from Ta atoms. Interestingly, the Ta peak position is apparently dependent on α. High background at lower energy at about 800 eV is caused by the Li^+ ion coming from deeper layers due to multiple scattering. Figure 2(b) shows the energy spectra of Li^+ ions obtained along the $[11\bar{2}0]$ azimuth at incident angles from 20° to 100° by a 5° step. The Ta surface peak positions are shifted to a lower energy side by decreasing or increasing the incidence angle from $\alpha = 75°$, and the value of the loss energy relative to the binary collision energy (863 eV) reaches more than 40 eV. The origin of the peak shift to the lower energy side is discussed later.

The polar angle scans of integrated Ta peak intensities along the $[10\bar{1}0]$ azimuth are shown by the open circles in Fig. 3(a). The α scans show two shadowing-focusing peaks. If the surface is terminated by the Ta atom, the shadowing critical angle must be about $\alpha = 14°$, as estimated from the shadowing of the Li^+ ion on the Ta chain with a distance of 5.4 Å along the $[10\bar{1}0]$ direction. The absence of such shadowing-focusing peaks at about $\alpha = 14°$ in the ICISS polar angle scans shows that the Ta is not shadowed by the adjoining Ta atom in the some plane but by the B atom. The relatively larger shadowing critical angle ($\sim 60°$) indicates that B is located above the Ta plane (B termination of the surface).

The polar angle scans of the integrated Ta surface peak intensity were obtained along the $[11\bar{2}0]$ azimuth and the results are shown in Fig. 3(b). In contrast to the results taken along the $[10\bar{1}0]$ azimuth, a strong Li^+ intensity is obtained even at small incidence angles. Note that a steep cutoff of the Ta peak intensity exists at $\alpha = 21°$. The critical angle of $\alpha = 21°$ in Fig. 3(b) is explicable by the shadowing effect of the in-plane Ta atoms along the $[11\bar{2}0]$ azimuth, indicating that no shadowing of the first-layer B atoms takes place in this azimuth.

The above experimental facts are consistent with the ideal structure of the B-terminated $TaB_2(0001)$ surface as shown in Fig. 1; the B atoms are located at the threefold hollow site forming a two-dimensional graphitic layer. The cross sections of the surface along $[10\bar{1}0]$ and $[11\bar{2}0]$ directions are shown in the inset of Fig. 3. The two main peaks of the ICISS α scan in Fig. 3(a) are caused by the shadowing and focusing effects of the B(1) atom on the Ta(1) atom ($\alpha = 60°$) and the blocking effect of the B(2) atom ($\alpha = 94°$) on the outgoing trajectory. The atomic position of the first-layer B relative to the second-layer Ta is determined from the experimental shadowing critical angles ($\alpha = 60°$) by using the shadow cone of B which is calculated using the Thomas-Fermi-Moliere potential with a reduced Firsov's screening length factor of 0.7. The spacing between the outermost B layer and

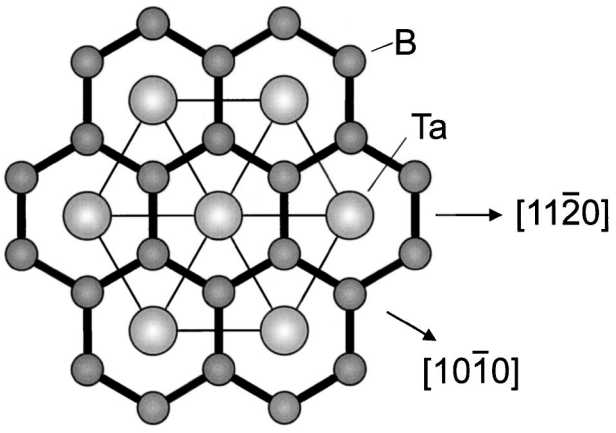

FIG. 1. Projection along the [0001] azimuth of TaB_2.

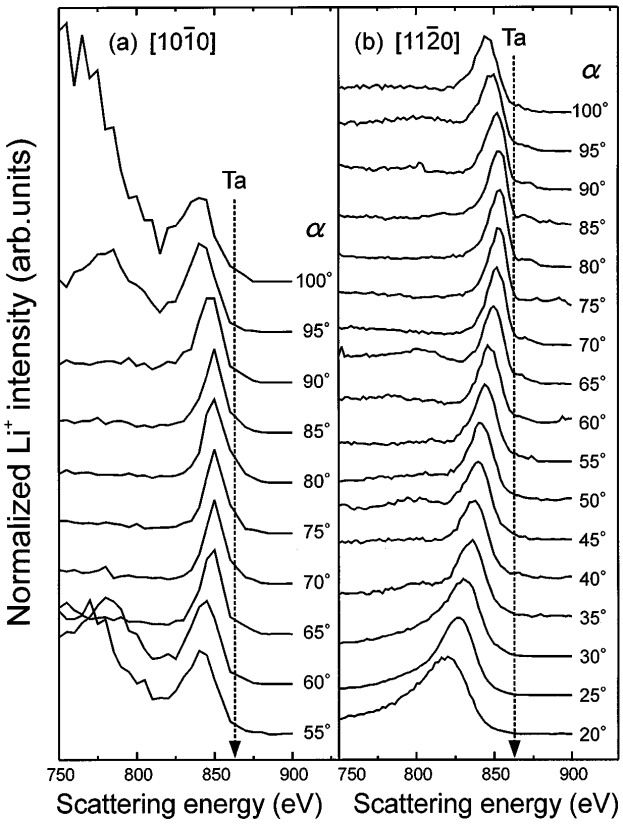

FIG. 2. Energy spectra of Li^+ scattered from $TaB_2(0001)$ with various incident angles; the measurements were made with 1 keV Li^+ ions along the (a) $[10\bar{1}0]$ and (b) $[11\bar{2}0]$ azimuth at the fixed scattered angle of 155°. The energy position for elastic binary collision of Li on Ta is indicated by an arrow. The peak heights were all normalized to be the same.

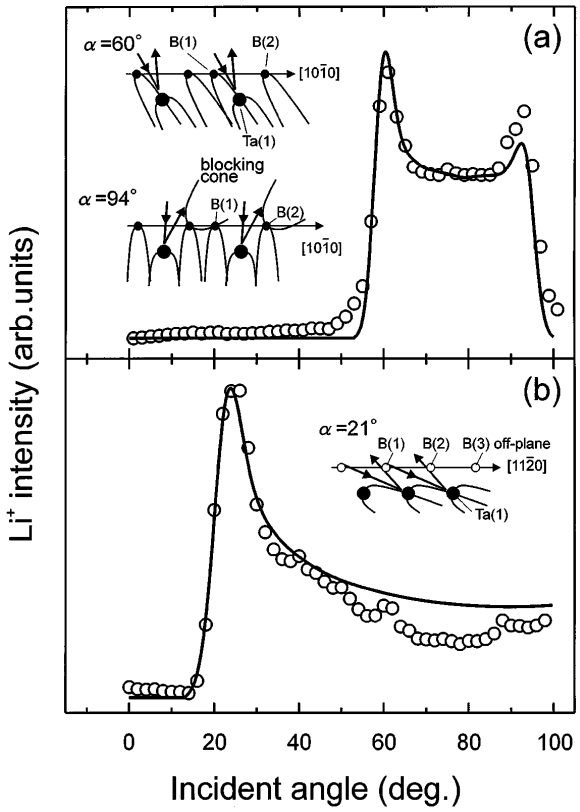

FIG. 3. Open circles: the integrated α scan of Li^+-ICISS; solid lines: simulated intensity with scattering energy of 860 eV obtained using the 3D3A model along (a) the $[10\bar{1}0]$ azimuth and (b) the $[11\bar{2}0]$ azimuth. The insets show schematic views of the shadow and blocking cones for $E_0 = 1\,\mathrm{keV}$ Li^+ ions together with the side views of $TaB_2(0001)$.

the second Ta layer is thus determined as 1.75 ± 0.02 Å, which is larger than that of the bulk TaB_2 crystal (1.61 Å) by 8.47%. Along the $[11\bar{2}0]$ azimuth, the critical angle of $\alpha = 21°$ corresponds to the shadowing effect on the Ta chain, where the Li^+ ions can penetrate into the second layer through the outermost-layer B arrays, as shown in the inset of Fig. 3(b).

With respect to the electronic property, two distinct charge transfer models for the transition-metal diborides have been proposed. One is the charge transfer from the metal to the boron [15], and the other is the opposite [16]. Both models suppose the hybridization between the boron and metal orbitals. The former model, based on the band structure calculations of simple and transition-metal diborides, indicates that the B^- negative ions form graphitic networks and that the band structure is similar to graphite. However, the graphitic bands are strongly modified by the hybridization between the boron and metal orbitals in TiB_2 [15]. Hayami *et al.* have reported surface structures of $HfB_2(0001)$ using ICISS. It is shown that the Hf layer terminates the surface and the B atoms desorb even from the second layer above 2300 K [17]. The critical difference in the surface termination between the HfB_2 and TaB_2 surfaces should be related to the number of d electrons since dominant bonding between boron and metal is due to the hybridization of boron p and metal d states. In the case of the TaB_2, Ta has one more d-orbital electron than Hf, so that the bonding between B and Ta should be stronger than HfB_2. Thus, the B layer is stabilized and terminates the $TaB_2(0001)$ surface.

Work function (WF) of the $TaB_2(0001)$ as determined from the width of the UP spectra is 6.0 eV [18] which is much larger than that of polycrystal boron (4.5 eV). In the case of $LaB_6(100)$, the topmost layer of the $LaB_6(100)$ consists of La atoms, and the charge transfer from the La atoms to the B_6 clusters produces dipoles at the surface, thereby leading to the WF as low as 2.5 eV. The larger WF of the boron-terminated surface such as $TaB_2(0001)$, being the opposite case of the LaB_6, indicates that there is a charge transfer from the Ta to the B atoms.

The ICISS α scan intensities from the boron-terminated $TaB_2(0001)$ surface were further simulated by using three-dimensional three-atom (3D3A) model [19] which can reproduce shadowing and blocking effects; the scattering cross section is calculated using in-plane three atoms [B(1)-Ta(1)-B(2) for the $[10\bar{1}0]$ azimuth and the liner Ta chain for the $[11\bar{2}0]$ azimuth]. The calculated results, assuming the above-obtained Ta-B spacing, are shown by the solid lines in Fig. 3. The simulated results at an energy of 860 eV are in good agreement with the experiment of the integrated α scan. In order to obtain the best fit to the experimental results, the calculated scattering cross section is broadened by a Gaussian distribution function. From the focusing peak width, therefore, thermal vibration amplitude of the $TaB_2(0001)$ surface can be estimated. The root mean square displacement perpendicular to the surface of the Ta in the second layer, $\langle u_\perp^2 \rangle^{1/2}$, is obtained as 0.08 Å, which corresponds to the Debye temperature of $\Theta_\perp = 370\,\mathrm{K}$.

As far as the scattering cross sections are concerned, computer simulation reproduces experimental ICISS intensities, including shadowing and blocking peaks, quite nicely. However, the simulation cannot reproduce the incident-angle dependence of the Ta surface peak position as seen in Fig. 2. In general, the scattered particles from the surface lose their energy due to the recoiling of target atoms (nuclear stopping) and excitation of electron-hole pairs (electronic stopping). The 3D3A model is based on the consecutive diatomic collision model including the recoil of target atom, but electronic stopping is ignored. Hence, the origin of the Ta peak shifts toward the lower energy side, as seen in Fig. 2, should be ascribed to electronic stopping.

Figure 4 shows the trajectory and incident energy dependence of inelastic energy loss of the Ta surface peaks along the $[11\bar{2}0]$ azimuth. It is well known that the energy loss due to electronic stopping (nuclear stopping) is proportional to the square root of (linear to) the kinetic energy. As shown in the inset, the energy loss value is proportional to the square root of the incident ion energy at every incident angle. In the very low energy regime

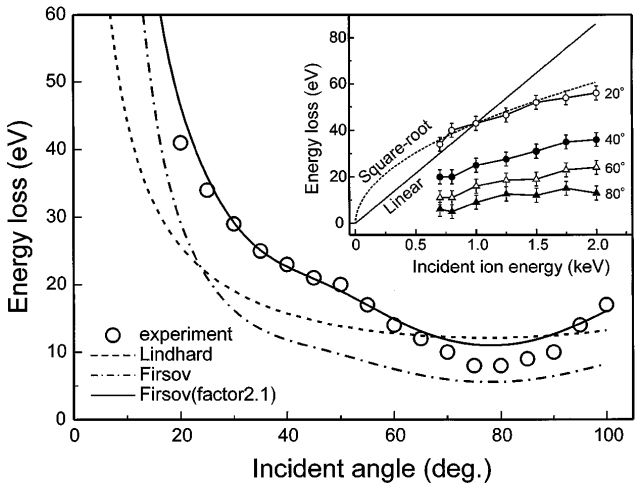

FIG. 4. Incidence-angle dependence of the inelastic energy loss of $E_0 = 1$ keV Li^+ ions scattered from the $TaB_2(0001)$ surface taken along the $[11\bar{2}0]$ azimuth at a fixed scattering angle of 155°. The experimental result (open circles) are compared to the theoretical stopping powers proposed by Lindhard and Firsov. The inset shows incident ion energy dependence of the scattered Li^+ ion energy loss along the $[11\bar{2}0]$ azimuth at a fixed scattering angle of 155°.

below 500 eV, the electronic stopping is known to be more complicated and deviates from linear or square root dependence [20]. However, in the present experiment the situation is much simpler as evidenced in Fig. 4 and energy loss is basically electronic stopping in nature.

The theories of the electronic stopping are proposed by Firsov [21] and Lindhard *et al.* [22]. Figure 4 shows the experimental electronic energy losses at $E_0 = 1$ keV, together with the calculated loss based on the Firsov and Lindhard models, as a function of the incident angle. Note that the experimental α scan of the energy loss has a small hump at about 47° and a minimum at about the specular angle of 78°. Both theories show significant energy loss at a shallower incident angle and a minimum at the specular angle. A small hump of about 47° is reproduced by the Firsov theory but not by the Lindhard theory. This is because the Firsov equation has an impact parameter dependence. The hump arises when the incident Li^+ ions pass the off-plane B(2) pair at $\alpha = 47°$, which corresponds to the direction along B(2)-Ta(1) in the inset of Fig. 3(b). The Li^+ ions also lose their kinetic energy on the outgoing trajectory with the influence of the B(2) pair at $\alpha = 21°$. Thus the loss energy of Li^+ ions increases with the decrease of the incident angle. The incoming and outgoing trajectories of the Li^+ ions at the specular angle of $\alpha = 78°$ are far from the neighboring boron pairs, B(2) and B(3), and, hence, the energy loss of Li^+ ions goes into a minimum. The energy loss of scattered Li^+ ions increases again with the increase of the incident angle, because the Li^+ ions on the outgoing trajectory pass near the B(3) pair. The incident angle dependence of the energy loss is qualitatively reproduced by the impact parameter approximation proposed by Firsov. Quantitatively, however, the calculated energy loss of the electron momentum transfer to boron atoms is underestimated. A better fit between the Firsov model and the experimental result is obtained if the energy loss of the boron part in the Firsov model is simply multiplied by a factor of 2.1. This misfit between the Firsov model and the experiment may be caused by the electronic shell effect of both projectile and target atoms [23] which is ignored in the Firsov model based on the Thomas-Fermi potential. A more probable model may therefore be given by the molecular orbital calculation [24]. In this picture, since the B $2p$ (Li $1s$) orbital has antibonding (bonding) character during collision, electronic stopping relates mainly to the excitation of the B $2p$ electrons. Therefore a larger value of electronic stopping arises from the negatively charged B atom.

The authors are grateful to W. Hayami for the use of his 3D3A simulation code, and to T. Aizawa and M. Kato for helpful discussions.

[1] *Boron and Refractory Borides*, edited by V. I. Matkovich (Springer, New York, 1977).
[2] Boron-Rich Solids, D. Emin *et al.*, AIP Conf. Proc. No. 231 (AIP, New York, 1990).
[3] H. Ihara, M. Hirabayashi, and H. Nakagawa, Phys. Rev. B **16**, 726 (1977).
[4] R. L. Johnson, B. N. Harmon, and S. H. Liu, J. Chem. Phys. **73**, 1898 (1980).
[5] T. Tanaka, Y. Ishizawa, E. Bannai, and S. Kawai, Solid State Commun. **26**, 879 (1978).
[6] R. Nishitani *et al.*, Surf. Sci. **93**, 535 (1980).
[7] J. S. Ozcomert and M. Trenary, Surf. Sci. **265**, L227 (1992).
[8] J. S. Ozcomert and M. Trenary, Chem. Mater. **5**, 1762 (1993).
[9] N. Yamamoto *et al.*, Surf. Sci. **357-358**, 708 (1996).
[10] T. Aizawa, R. Souda, S. Otani, and Y. Ishizawa, Phys. Rev. Lett. **64**, 768 (1990).
[11] A. Nagashima *et al.*, Phys. Rev. Lett. **75**, 3918 (1995).
[12] S. Zaima, Ph.D. thesis, Tohoku University, 1982 (unpublished).
[13] W. Hayami *et al.*, Jpn. J. Appl. Phys. **10**, 172 (1994).
[14] S. Otani and T. Tanaka (to be published).
[15] A. J. Freeman *et al.*, *Surface Properties of Layered Structures*, edited by G. Benedek (Kluwer, The Netherlands, 1992) p. 97.
[16] V. M. Anishchik and N. N. Dorozhkin, Phys. Status Solidi (b) **160**, 173 (1990).
[17] W. Hayami (private communication).
[18] H. Kawanowa, R. Souda, S. Otani, and Y. Gotoh (to be published).
[19] W. Hayami *et al.*, Surf. Sci. **303**, 247 (1994).
[20] T. Kaneko, Surf. Sci. **236**, 203 (1990).
[21] O. B. Firsov, Sov. Phys. JETP **36**, 1076 (1959).
[22] J. Lindhard and M. Scharff, Phy. Rev. **124**, 128 (1961).
[23] I. M. Cheshire, G. Dearnaley, and J. M. Poate, Phy. Lett. **27A**, 304 (1968).
[24] M. Kato (to be published).